International Journal of Modern Manufacturing Technologies
ISSN 2067–3604, Vol. XVII, No. 3 / 2025
https://doi.org/ 10.54684/ijmmt.2025.17.3.151

# DESIGN AND CONSTRUCTION OF A BENCH FOR PCB PANEL TESTING AND DEPANELIZATION

**Mateusz Łyczek[1,2], Wojciech Skarka[3]**

[1,3]Silesian University of Technology, Akademicka 2A, 44-100 Gliwice, Poland
[2]AIUT Sp. z o.o., Leona Wyczółkowskiego 113, 44-109 Gliwice, Poland

Corresponding author: Mateusz Łyczek, mlyczek@polsl.pl

***Abstract:*** Today's world is increasingly relying on electronic products in everyday life, and the advancement of modern technologies. Electronics have become essential in a variety of industries, including medicine, communications, transportation, and entertainment. The basic element of electronic devices is the printed circuit board (PCB), which ensures the stability and proper functioning of electrical systems. As such, the quality and precision of PCB manufacturing are critical to the reliability and durability of electronic devices.
The PCB manufacturing process is complex and multi-stage, and quality control plays a vital role in eliminating manufacturing defects. Advanced testing and depanelization technologies are used to achieve maximum precision, separating individual boards from larger production panels. Modern test benches are essential to ensure consistency and reliability in production, enabling automatic defect detection and analysis of component parameters.
This article introduces the design and construction of an advanced test bench for testing and depanelizing PCB panels. The main objective of the research was to assess the accuracy of the positioning of the system in different modes of operation and under variable loads. The measurements were made with a high-precision laser sensor P-450-M12 from LEUZE. The analysis showed that the largest deviations occurred in the X-axis, where both the mean and maximum values of MEA errors exceeded the assumed thresholds (0.5 mm and 1–2 mm). Better results were achieved in controlled modes (Smooth and Sectional), especially in the Y and Z axes, confirming the potential of the system as a prototype.
Identified sources of problems include, among others, mechanical play, structural susceptibility to vibration, and suboptimal distribution of the center of gravity. In addition, the influence of ambient conditions (e.g., sunlight) on the accuracy of limit sensors was noted. Despite the lack of vibration damping and advanced filtering, the system demonstrated measurement stability under laboratory conditions.
The stand currently serves as a prototype proof-of-concept demonstrator and provides a solid basis for further development. Structural modifications, automation of the analysis process, and integration with vision systems are planned. The obtained results do not directly increase the precision, efficiency, or reliability of industrial solutions, but they indicate design directions and potential approaches that can be used in the development of future industrial PCB production systems with higher precision and reliability.

***Key words:*** Cartesian robot, mechatronics, diagnostic PCB, depanelization PCB, CAD design

## 1. INTRODUCTION

The modern world is increasingly based on electronic devices that are used both in everyday life and in advanced industrial, military or scientific systems. A common element of all these devices is printed circuit boards (PCBs), which are the basis for the functioning of electronic circuits. A printed circuit board is made of a non-conductive substrate, mostly made of composite materials such as epoxy or fiberglass, and conductive copper traces that connect the individual components.
Due to its design, PCBs can be classified based on the number of layers and the rigidity of the structure [1]. Single-layer, double-layer, and multilayer boards are available, as well as rigid, flexible, and hybrid (rigid-flexible) substrates. This classification is presented in Table 1, while schematic cross-sections of boards with different numbers of layers are illustrated in Figure 1.
Figures 1–5 are reproduced from our earlier publication [2], published under the CC BY 4.0 license, which allows unrestricted reuse with attribution.

Table 1. Division of PCBs [1].

| **Division of PCBs** | | | | | |
|---|---|---|---|---|---|
| **Due to the number of layers** | | | Due to the stiffness of the insert | | |
| **Single-layer** | Double-layer | Multi-layer | Rigid | Flexible | Rigid-Flex |

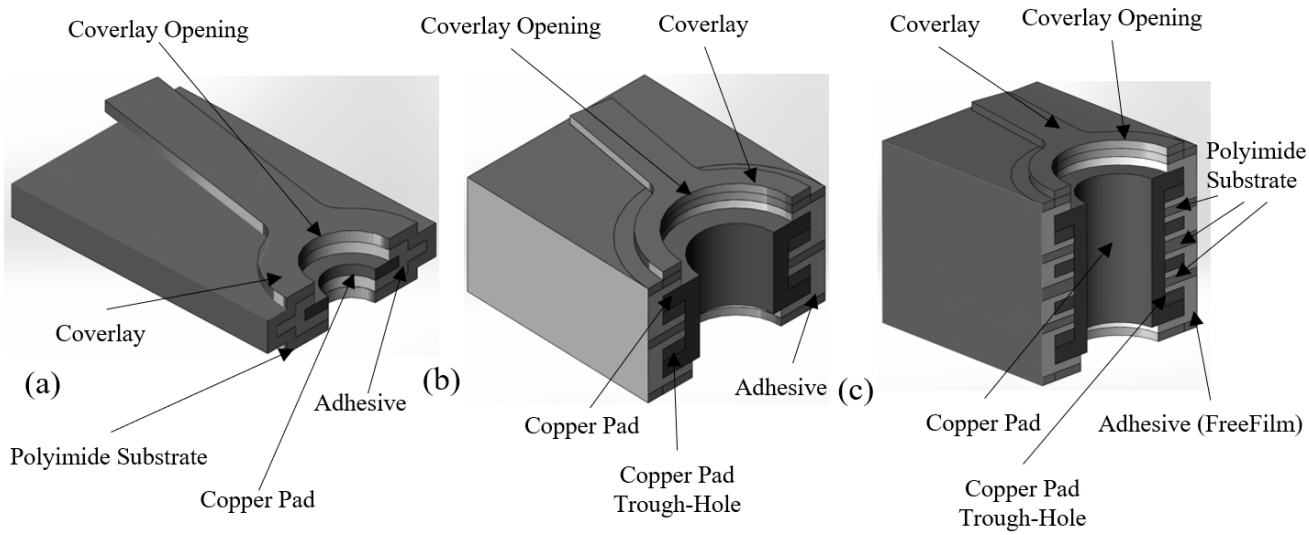


Fig. 1. Cross sections of rigid PCBs in terms of the number of layers: (**a**) single-layer PCB, (**b**) double-layer, (**c**) multi-layer (reproduced from [2], CC BY 4.0).

In order to increase production efficiency, PCBs are combined into assemblies called panels. Panelization allows for the assembly of more systems in one cycle, which significantly affects the speed and economics of the production process. In addition, the panels facilitate the standardization of the dimensions of elements assembled on automatic lines, which is especially important in the case of irregularly shaped tiles [3]. The most commonly used methods of connecting boards in panels include V-scoring and tab-routing.
V-scoring involves making two parallel V-shaped cuts on both sides of the panel. Some of the material is removed, leaving behind a thin layer that binds the tiles together. This layer is strong enough to hold the entire panel together while still allowing the components to be easily separated. This method is mainly used for rectangular or square-shaped tiles. The second method is lap milling, which involves milling the area around each wafer, leaving fragments of material (so-called bridges) in which perforations are made - the so-called "Mouse Bite". This solution is dedicated to tiles with more complex, irregular shapes. Both methods are shown in Figure 2 and Figure 3.

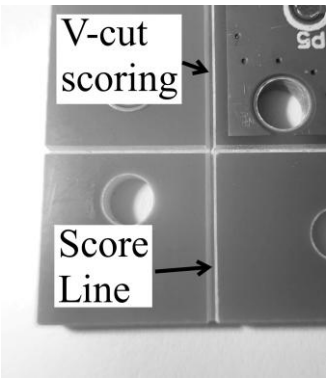


Fig. 2. Types of connections between boards in a PCB panel - V-scoring (reproduced from [2], CC BY 4.0).

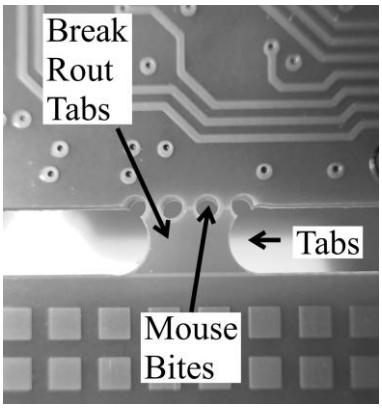


Fig. 3. Types of connections between boards in a PCB panel - Tab-routing (reproduced from [2], CC BY 4.0).

After the installation is completed, the necessary stage is depanelization, i.e., separating individual tiles from the panel. This is often done by hand, using tools such as side pliers or pliers. However, manual depanelization

carries the risk of damaging the board - from mechanical damage to components, through cracks in conductive paths, to the formation of imperfections on the edges. Such damage may negatively affect the further assembly of the board in the housing or its subsequent functioning. An example of such an imperfection is shown in Figure 4 [4],[5].

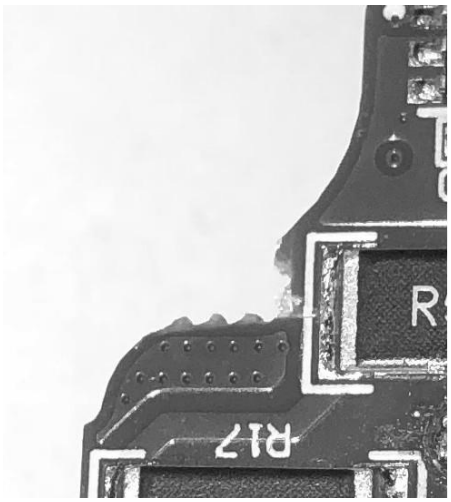


Fig. 4. An imperfection left on the perimeter of the PCB (reproduced from [2], CC BY 4.0).

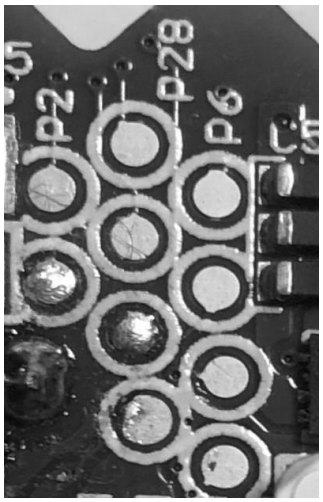


Fig. 5. Test pads on PCB (reproduced from [2], CC BY 4.0).

Diagnostics of PCBs and entire panels is a crucial step in the manufacturing process of electronic devices and should not be overlooked. Systematic testing allows you to reduce production costs, comply with industry standards and ensure the quality of the final product. One of the basic diagnostic methods is the In-Circuit Test (ICT), which allows you to check the correctness of component assembly by measuring currents and voltages at selected test points, the so-called pads. These points are designed in appropriate locations on the circuit board to allow easy access to the test probes. An example of the arrangement of the test electrodes is shown in Figure 5.
The concepts of depanelization and PCB diagnostics are explained above, and some of the methods used in these processes are described below. Many examples can be found in the literature, but a paper presenting an overview of these issues is particularly valuable [2]. The authors divided the techniques into several categories and discussed the relevant publications related to each approach. Some of the research focused on the use of vision systems and image processing, supported by neural networks learning to interpret photos [6],[7]. The diagnostic method of the "flying probe", known since 1987, was also presented. It involves the use of probes mounted on movable arms, enabling fast and precise positioning on test pads. Currently, an analysis of the damage to the probes themselves is being m.in developed [8]. Another method is "BED OF NAILS", which involves testing the functionality of the entire board using an additional electronic circuit. The parameters of individual components [9], [10] are checked, and this technique is mainly used for small boards [11]. It is also worth mentioning two less popular, but interesting approaches. One of them uses ultrasound at a frequency of 2 MHz to detect component damage [12], the other is Interconnect Stress Testing (IST), examining the integrity of connections using current flowing through specially designed paths [13]. PCB panel depanelization can be divided into two main methods: milling/drilling and laser processing. Several scientific articles refer to this division. One article used QFD analysis to determine the technical requirements for building a machine that can act as a PCB depanelization machine [14], and another shows how to build an affordable milling machine from commercially available components [15]. In the case of laser processing, the focus was mainly on the selection of laser parameters depending on the thickness of the wafer and its impact on the quality of the final product [16]s.
This study is a summary of the design and research work of a substation that integrates the testing and depanelization functions of PCB circuits into its design. The test functions are carried out using a "bed of nails" mounted on a Cartesian robot. In contrast, depanelization functions are performed using the PLH3D-XT8 laser head, also mounted on a Cartesian robot. The study aimed to analyse the accuracy of the PCB testing and depanelization station. The information collected will serve as a starting point for further analysis and development of innovative technological solutions in this area.

## 2. MATERIALS AND METHODS

### 2.1. Description of the Test Stand

The research was carried out on a mechatronic system with a Cartesian design, equipped with four independently controlled linear axes (LASER Y, Z; TESTER Y, Z). Each of the axes is based on ball screws and linear guides, which ensures high rigidity and repeatability of movement. The Z axis offers 200 mm of travel, and the Y axis 500 mm. To move the X axes of the LASER and TESTER, a special drive has been designed consisting of a nut for the linear screw connected to the stepper motor by a corresponding gear ratio of 1:1. Figure 6 shows a model of such a drive. In this drive, the ball screw has all degrees of freedom removed, while the ball nut rotates and moves along its axis. The drive is carried out by 23HS45-4204D-E1000 stepper motors. Each axis has a permanently mounted limit sensor in the extreme position.

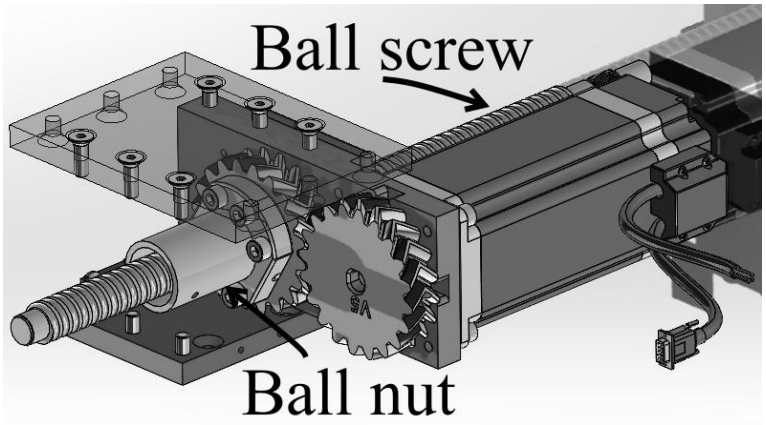


Fig. 6. Screenshot of X-axis drive model.

Instead of blocking the movement of the axis itself, the limit sensor detects the end position of the moving element. When the sensor is triggered, the control software stops further motion in that direction to prevent mechanical collision. The sensor also provides a reference signal used during the homing procedure to define the zero point of each axis. The next task of the sensor was to determine the "0" point of each axis. The process of calibrating the axes and saving the corresponding parameter was performed. The motion is controlled by a Raspberry Pi 5 single-board computer, working with CL57T-V4.1 digital stepper motor controllers. The entire drive system and user interface has been developed in the Python environment, allowing control of each axis of the mechatronic system. The power supply of the system is provided by an external 36V switching power supply. The measurement is carried out by controlling the movement of the axes in the following modes: smooth motion, segmental motion and random motion. These modes will be described later in the article. The measuring system consists mainly of the ODS9L2.8/LAK laser rangefinder. P-450-M12. It allows you to read the actual position with an accuracy that allows you to analyse errors in the order of tenths of a millimetre. On the other hand, its reach from 50 to 500 mm perfectly matches the range of the tested axles sensors

The laser was mounted each time so that the data could be easily read. For mechanical reasons, the type of obstacle from which measurements were to be counted was mounted at the other end of the sensor indicator. Figure 7 shows a rangefinder mounted on the Z-axis.

In the further part of the work, visualizations of the measuring station are presented, which are aimed at illustrating both the actual measurement system and its design concept. Figure 8 shows a screenshot from SolidWorks showing a 3D model of the workstation that formed the basis for designing its physical version. This model enabled the initial verification of the correctness of assembly and geometry of the system, which was helpful at the stage of planning the experiment. The photo highlights elements such as: stepper motor, test head, laser head, structural element and linear guide. Figure 9 shows a projection showing the mechatronic control panel.

Fig. 7. Representation of the Z-axis with a rangefinder mounted.

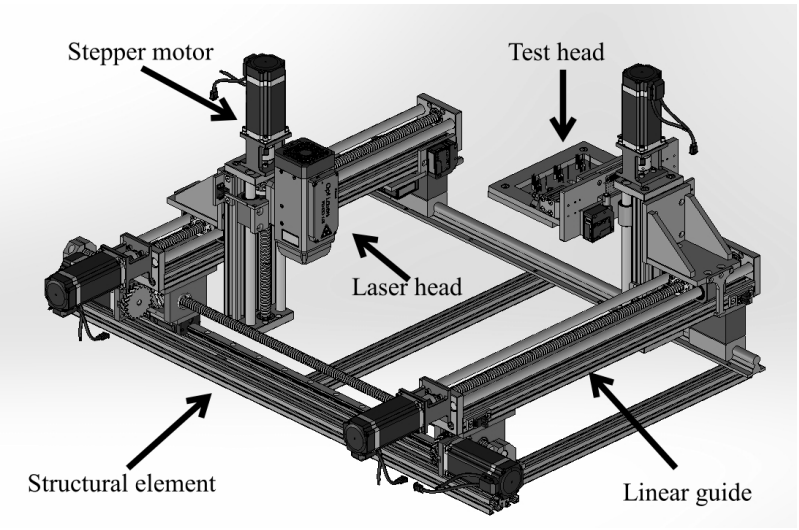


Fig. 8. Screenshot of Cartesian Robot Design for PCB Panel Diagnostics and Depanelization.

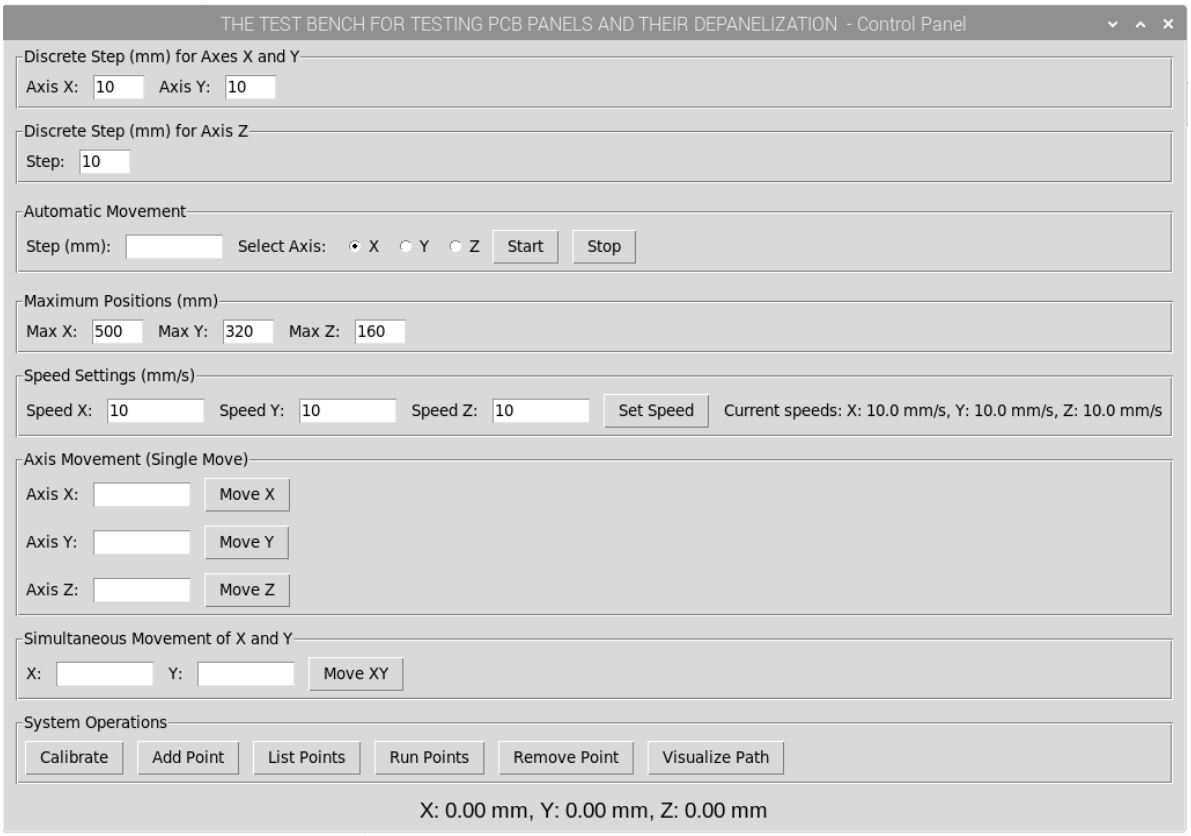


Fig. 9. Screenshot of Cartesian Robot Control Panel for PCB Panel Diagnostics and Depanelization.

## 2.2. Measurement methods

Before starting the actual series of measurements, the correctness of the laser rangefinder readings was verified. For this purpose, its readings were compared with measurements made with a digital caliper. Reference points were set manually, and then the distances between the individual positions of the head were measured. The readings from the rangefinder were compared with the values obtained with the caliper. The analysis showed a very good compatibility of both measurement methods, which confirmed the suitability of the rangefinder for further position recording in dynamic tests. This made it possible to use it as a primary measuring tool without the need for additional calibration.

### 2.3. Research methodology

The study aimed to analyse the displacement accuracy of the moving elements in the mechatronic system depending on the selected motion-control configuration. The main objective was to determine how the number of steps per millimetre (steps/mm) affects the precision of movement along the X, Y, and Z axes.

The need for this analysis arose during preliminary verification of the system. During initial tests it was observed that after executing a programmed movement, the position of the moving element did not coincide with the reference value indicated by the rangefinder. The discrepancies were visible to the naked eye and reached approximately 1-3 mm over a distance of 100 mm, even though no actuators, such as the laser or tester, were installed at that stage. This suggested that the actual number of steps per millimetre differed from the value resulting from the mechanical design.

The measurements were performed for two mechanical systems referred to as LASER and TEST. Both the unloaded configuration and the configuration with an additional load on the Z-axis (caused by the mounted actuator) were examined. Each set of tests consisted of three types of displacement verification.

In the smooth test, the motion was carried out continuously over a distance of 0-160 mm for the Z-axis and 0-300 mm for the X and Y axes. Based on the relationship between the voltage from the measurement system and the rangefinder reading, a linear function was determined and later used to convert data in the following tests:

- Smooth test: the motion was carried out continuously between two fixed positions over a distance of 0-160 mm for the Z axis and 0-300 mm for the X and Y axes. Because the movement in this test was uninterrupted and involved only the initial and final positions, the measurement system provided two reference values corresponding to these points. These values were used to determine the linear conversion function between the measured voltage [V] and the rangefinder indication [mm]. The function served only as a calibration step and was then applied in the subsequent sectional and random tests, in which the actual assessment of linearity and correlation was performed based on multiple measurement points.
- Sectional test: Movement was performed in increments of a specified section (e.g., every 25 mm), and positions were measured at each stopping point. For the Z axis, sections of 80 mm, 40 mm, 20 mm, 10 mm, and 5 mm were tested, while the X and Y axes were measured every 150 mm, 100 mm, 50 mm, 25 mm, 10 mm, 7.5 mm, and 5 mm. Each segment length produced a separate measurement series, and because each series contained its own set of discrete points, an individual linear regression and correlation coefficient were calculated for every division. For the Z-axis of the LASER system, all series showed a very high level of linearity between the programmed position and the rangefinder indication. Due to the negative slope of the regression line, the correlation coefficients take negative values, with magnitudes close to 1 (for example, $|R| \approx 0.999$ for the 80 mm series). The obtained voltage values were then used to calculate the rangefinder indication using the previously determined linear function. These indications were compared with the programmed values, allowing for an initial assessment of systematic error and repeatability.
- Random test: the system moved to up to 20 randomly generated positions. These positions were produced in the control script using the random uniform function. The generated values were limited to the working range of the axis and rounded to 0.1 mm so they could be used directly by the motion controller. After reaching each target point, the system waited 2 seconds before recording the sensor reading. The data analysis followed the same procedure as in the sectional test.

For each test, data was recorded in the form of: the set position, the sensor reading (rangefinder), the difference from the previous measurement, and the deviation from the expected value. The data were analysed in terms of: mean absolute error (MEA), maximum error, standard deviation and deviation of the angle of movement ($\Delta\alpha$) with respect to the ideal angle of -45° (this is the angle created by the linear function for the ideal reconstruction of the position, where the set of arguments X is the indication of the rangefinder, and the set of values of Y is the given program position). A string of 10 trials was performed for each test. After each trial, appropriate Charts were prepared that visualized the relevant data. Only sample charts will be presented below, as not all of them will fit into the article.

The selection of successive values of the number of steps per mm was calculated from smooth tests from the following formula (1).

$$n_{i+1}=(n_i \cdot S_p)/S_r \quad (1)$$

where: $n_{i+1}$ – new value of the steps per mm parameter; $n_i$ – current value of steps per mm; $s_p$ – distance set in the program [mm]; $s_r$ – average real distance travelled by the axle [mm] (average calculated from 10 attempts)

The general course of the examination of each axis was as follows. At the beginning, the LASER system was tested. The order of measurements was fixed: first the Z axis, then the Y axis, and finally the X. Initially, all tests were carried out without the actuator mounted on the Z axis. In the first step, the value of the number of steps per mm resulting from the mechanical design was entered - 200 steps per revolution of the motor and 5 mm travel per revolution of the ball screw, which gave 40 steps per mm. This value was entered into the control program. Then the SMOOTH test was performed - each time in 10 trials, with each test starting with the calibration of the zero position of the axis. After the end of this series, a new parameter value was calculated based on the data obtained. However, before it was introduced, the accuracy of the currently used setting was checked by performing a SECTIONAL and RANDOM test (also 10 runs each). Only after they were completed were the steps per mm parameter updated and the next test cycle began. If the new value differed from the previous value by less than ±0.05 steps per mm, it was considered final and saved as appropriate for further use. After the unloaded tests were completed, the actuator (laser) was assembled, and all tests were repeated. In this case, the final fixed value of the parameter was taken as a reference point. Other studies were carried out in a similar way. The TEST circuit (for testing PCBs) was tested immediately with the actuator mounted. The final parameters obtained for the corresponding axes in the LASER system were used as a reference value. This was due to the fact that the X, Y and Z axes are structurally identical in both systems.

## 3. RESULTS AND DISCUSSIONS

The main objective of the study was to determine the optimal parameter "steps/mm" for each axis of the Cartesian system. The measurements were based on the LEUZE laser sensor and its validation under real conditions. The process involved three test steps: Smooth, Sectional and Random, which differed in the methodology of movement and in the method of evaluating positional deviation. Each study looked at mean absolute error (MEA), maximum error, standard deviation, and the difference between the angle α and the ideal angle of -45° (denoted as Δα). Data was collected for three axes (X, Y, Z), two systems (LASER and TEST) and variants with and without load. Table 2 presents the aggregate results of these measurements. The optimal steps/mm value was determined by minimising the mean absolute error (MEA), standard deviation and |Δα|. All statistical values (MEA, maximum error, standard deviation, α and Δα) were calculated in Microsoft Excel using standard analytical and regression functions. The final value was accepted once further iterations changed the parameter by less than ±0.05 steps/mm and did not improve any of the evaluated metrics. The applied load corresponds to the mass of the actuator modules: the laser module (1.23 kg) and the tester module (2.5 kg). This additional mass was taken into account when comparing unloaded and loaded configurations.

Table 2. Summary table with test results [author's own work].

| Arrangement | Load | Axis | Steps/mm | Test Type | MEA [mm] | Maximum error [mm] | Standard deviation [mm] | α calculated | α perfect | Δα |
|---|---|---|---|---|---|---|---|---|---|---|
| **LASER** | Without | X | 40 | Smooth | 1.45 | 2.66 | 1.47 | -44.747 | -45.000 | -0.253 |
| **LASER** | Without | X | 40 | Sectional | 0.89 | 2.13 | 1.08 | -44.927 | -45.000 | -0.073 |
| **LASER** | Without | X | 39.65 | Smooth | 0.23 | 0.41 | 0.21 | -44.961 | -45.000 | -0.039 |
| **LASER** | Without | X | 39.65 | Sectional | 0.51 | 1.02 | 0.52 | -44.982 | -45.000 | -0.018 |
| **LASER** | Without | X | 39.65 | Random | 1.15 | 2.97 | 0.89 | -45.037 | -45.000 | 0.037 |
| **LASER** | Without | Y | 40 | Smooth | 1.95 | 3.56 | 1.96 | -44.662 | -45.000 | -0.338 |
| **LASER** | Without | Y | 40 | Sectional | 0.75 | 1.86 | 0.89 | -44.678 | -45.000 | -0.322 |
| **LASER** | Without | Y | 39.66 | Smooth | 0.47 | 0.83 | 0.47 | -44.921 | -45.000 | -0.079 |
| **LASER** | Without | Y | 39.66 | Sectional | 0.64 | 1.62 | 0.82 | -44.949 | -45.000 | -0.051 |
| **LASER** | Without | Y | 39.55 | Smooth | 0.93 | 1.69 | 0.92 | -44.844 | -45.000 | -0.156 |
| **LASER** | Without | Y | 39.55 | Sectional | 0.62 | 1.80 | 0.74 | -44.972 | -45.000 | -0.028 |
| **LASER** | Without | Y | 39.55 | Random | 5.24 | 12.43 | 3.36 | -46.002 | -45.000 | 1.002 |
| **LASER** | Without | Y | 39.33 | Smooth | 0.15 | 0.30 | 0.17 | -44.972 | -45.000 | -0.028 |
| **LASER** | Without | Y | 39.33 | Sectional | 0.20 | 0.57 | 0.27 | -45.018 | -45.000 | 0.018 |
| **LASER** | Without | Y | 39.33 | Random | 1.11 | 3.56 | 0.96 | -45.104 | -45.000 | 0.104 |
| **LASER** | Without | Z | 40 | Smooth | 1.51 | 2.74 | 1.50 | -44.513 | -45.000 | -0.487 |
| **LASER** | Without | Z | 40 | Sectional | 0.51 | 1.61 | 0.67 | -44.645 | -45.000 | -0.355 |
| **LASER** | Without | Z | 40 | Random | 0.93 | 3.16 | 0.81 | -44.659 | -45.000 | -0.341 |
| **LASER** | Without | Z | 39.33 | Smooth | 0.42 | 0.42 | 0.35 | -45.400 | -45.000 | 0.400 |
| **LASER** | Without | Z | 39.33 | Sectional | 0.49 | 1.46 | 0.65 | -45.096 | -45.000 | 0.096 |
| **LASER** | Without | Z | 39.33 | Random | 0.94 | 3.28 | 0.83 | -44.645 | -45.000 | -0.355 |
| **LASER** | Without | Z | 39.12 | Smooth | 0.04 | 0.07 | 0.04 | -44.988 | -45.000 | -0.012 |
| **LASER** | Without | Z | 39.12 | Sectional | 0.34 | 0.95 | 0.48 | -45.105 | -45.000 | 0.105 |

| | | | | | | | | | | |
|---|---|---|---|---|---|---|---|---|---|---|
| **LASER** | Without | Z | 39.12 | Random | 0.59 | 1.64 | 0.43 | -45.090 | -45.000 | 0.090 |
| **LASER** | Loaded | X | 39.65 | Smooth | 0.76 | 1.37 | 0.77 | -44.843 | -45.000 | -0.157 |
| **LASER** | Loaded | X | 39.65 | Sectional | 0.73 | 2.27 | 1.03 | -44.839 | -45.000 | -0.161 |
| **LASER** | Loaded | X | 39.65 | Random | 1.37 | 4.66 | 1.14 | -44.826 | -45.000 | -0.174 |
| **LASER** | Loaded | X | 39.43 | Smooth | 0.14 | 0.25 | 0.13 | -44.984 | -45.000 | -0.016 |
| **LASER** | Loaded | X | 39.43 | Sectional | 0.83 | 2.35 | 1.17 | -45.089 | -45.000 | 0.089 |
| **LASER** | Loaded | X | 39.43 | Random | 1.34 | 4.39 | 1.13 | -44.990 | -45.000 | -0.010 |
| **LASER** | Loaded | Y | 39.33 | Smooth | 1.35 | 2.43 | 1.32 | -45.233 | -45.000 | 0.233 |
| **LASER** | Loaded | Y | 39.33 | Sectional | 0.56 | 1.64 | 0.73 | -45.198 | -45.000 | 0.198 |
| **LASER** | Loaded | Y | 39.33 | Random | 1.41 | 3.48 | 0.97 | -45.267 | -45.000 | 0.267 |
| **LASER** | Loaded | Y | 39.65 | Smooth | 0.16 | 0.29 | 0.16 | -45.001 | -45.000 | 0.001 |
| **LASER** | Loaded | Y | 39.65 | Sectional | 0.56 | 1.54 | 0.72 | -45.006 | -45.000 | 0.006 |
| **LASER** | Loaded | Y | 39.65 | Random | 0.82 | 2.41 | 0.68 | -45.059 | -45.000 | 0.059 |
| **LASER** | Loaded | Z | 39.12 | Smooth | 0.66 | 1.21 | 0.66 | -44.783 | -45.000 | -0.217 |
| **LASER** | Loaded | Z | 39.12 | Sectional | 0.19 | 0.48 | 0.22 | -45.039 | -45.000 | 0.039 |
| **LASER** | Loaded | Z | 39.12 | Random | 0.88 | 2.10 | 0.56 | -45.140 | -45.000 | 0.140 |
| **LASER** | Loaded | Z | 39.42 | Smooth | 0.12 | 0.21 | 0.11 | -45.053 | -45.000 | 0.053 |
| **LASER** | Loaded | Z | 39.42 | Sectional | 0.12 | 0.33 | 0.23 | -45.031 | -45.000 | 0.031 |
| **LASER** | Loaded | Z | 39.42 | Random | 1.22 | 4.76 | 1.20 | -45.136 | -45.000 | 0.136 |
| **TEST** | Loaded | X | 39.43 | Smooth | 0.71 | 1.28 | 0.64 | -45.077 | -45.000 | 0.077 |
| **TEST** | Loaded | X | 39.43 | Sectional | 1.33 | 4.58 | 2.09 | -44.915 | -45.000 | -0.085 |
| **TEST** | Loaded | X | 39.43 | Random | 1.73 | 5.93 | 1.42 | -44.954 | -45.000 | -0.046 |
| **TEST** | Loaded | X | 39.59 | Smooth | 0.35 | 0.60 | 0.32 | -45.057 | -45.000 | 0.057 |
| **TEST** | Loaded | X | 39.59 | Sectional | 1.02 | 4.11 | 1.59 | -44.934 | -45.000 | -0.066 |
| **TEST** | Loaded | X | 39.59 | Random | 0.82 | 2.68 | 0.59 | -44.846 | -45.000 | -0.154 |
| **TEST** | Loaded | X | 39.68 | Smooth | 0.12 | 0.23 | 0.14 | -44.991 | -45.000 | -0.009 |
| **TEST** | Loaded | X | 39.68 | Sectional | 1.15 | 4.05 | 1.73 | -44.845 | -45.000 | -0.155 |
| **TEST** | Loaded | X | 39.68 | Random | 1.87 | 5.77 | 1.48 | -44.855 | -45.000 | -0.145 |
| **TEST** | Loaded | Y | 39.65 | Smooth | 1.58 | 2.86 | 1.58 | -45.275 | -45.000 | 0.275 |
| **TEST** | Loaded | Y | 39.65 | Sectional | 0.83 | 1.62 | 0.88 | -45.098 | -45.000 | 0.098 |
| **TEST** | Loaded | Y | 39.65 | Random | 0.86 | 3.45 | 0.70 | -45.108 | -45.000 | 0.108 |
| **TEST** | Loaded | Y | 40.03 | Smooth | 0.33 | 0.58 | 0.31 | -45.055 | -45.000 | 0.055 |
| **TEST** | Loaded | Y | 40.03 | Sectional | 0.84 | 1.80 | 0.95 | -44.903 | -45.000 | -0.097 |
| **TEST** | Loaded | Y | 40.03 | Random | 0.85 | 3.45 | 0.69 | -45.103 | -45.000 | 0.103 |
| **TEST** | Loaded | Y | 40.1 | Smooth | 0.06 | 0.11 | 0.06 | -45.012 | -45.000 | 0.012 |
| **TEST** | Loaded | Y | 40.1 | Sectional | 0.82 | 1.73 | 0.94 | -44.825 | -45.000 | -0.175 |
| **TEST** | Loaded | Y | 40.1 | Random | 1.33 | 3.58 | 0.86 | -44.855 | -45.000 | -0.145 |
| **TEST** | Loaded | Z | 39.42 | Smooth | 0.68 | 1.23 | 0.68 | -44.779 | -45.000 | -0.221 |
| **TEST** | Loaded | Z | 39.42 | Sectional | 0.45 | 1.49 | 0.64 | -45.221 | -45.000 | 0.221 |
| **TEST** | Loaded | Z | 39.42 | Random | 0.97 | 2.75 | 0.83 | -45.378 | -45.000 | 0.378 |
| **TEST** | Loaded | Z | 39.72 | Smooth | 0.06 | 0.11 | 0.06 | -45.019 | -45.000 | 0.019 |
| **TEST** | Loaded | Z | 39.72 | Sectional | 0.39 | 1.29 | 0.66 | -45.221 | -45.000 | 0.221 |
| **TEST** | Loaded | Z | 39.72 | Random | 0.84 | 2.22 | 0.60 | -45.362 | -45.000 | 0.362 |

Figure 10 shows the charts for the LASER Without Z 40 Smooth. These charts describe the dependence of the rangefinder indication on the voltage, the deviation of the actual value from the setpoint value in the program, and the comparison of the actual value to the rangefinder indication. From the last diagram, *the a-factor* of the linear function is obtained, which is then converted into an angle and comparable to/relative to the ideal angle of -45°.

Figure 11. shows the charts related to the LASER Without Z 40 Sectional. The charts show the deviations of the point from the programmed position and the comparison of the programmed position with the rangefinder indication for different axis divisions.

Figure 12. displays charts related to LASER Without Z 40 Random. The charts show the deviations of the point from the programmed position for the 4 test and for all tests, and the comparison of the programmed position with the rangefinder indication.

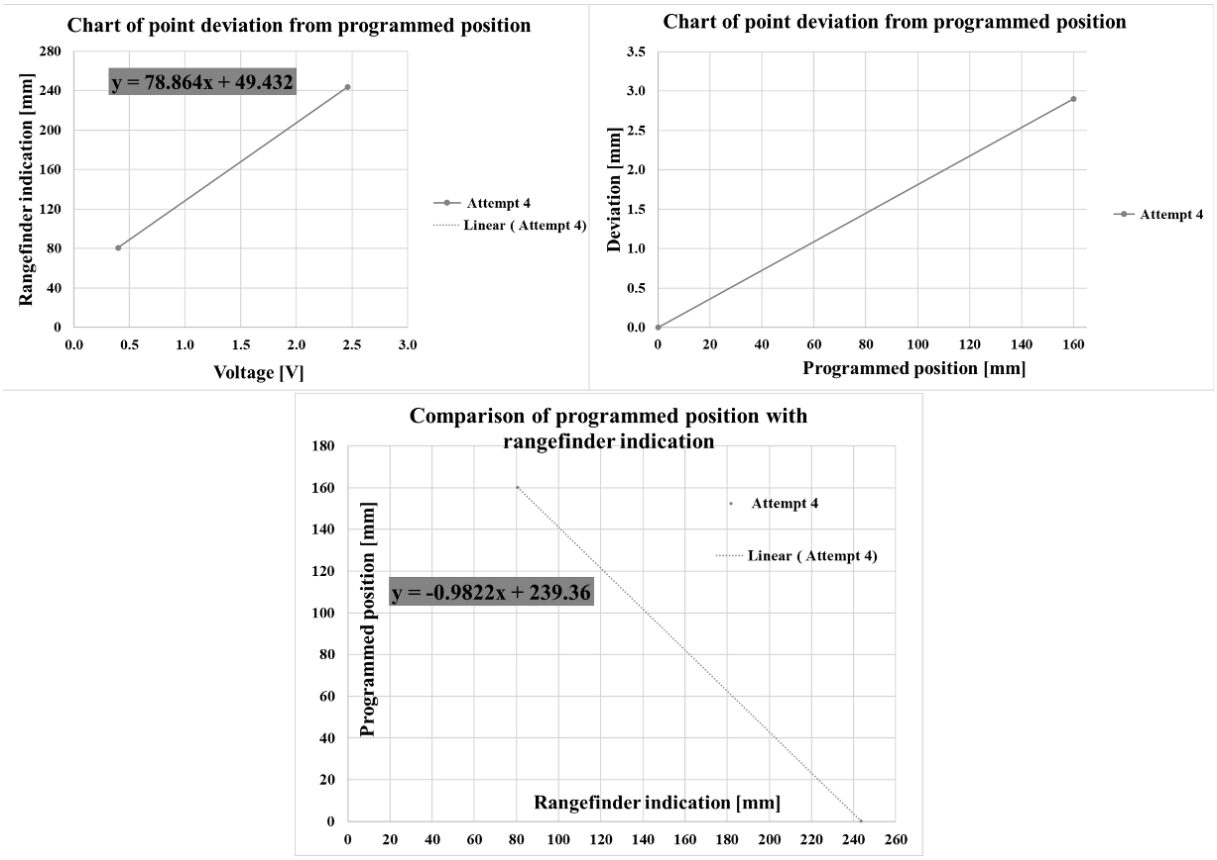


Fig. 10. Charts about LASER Without Z 40 Smooth.

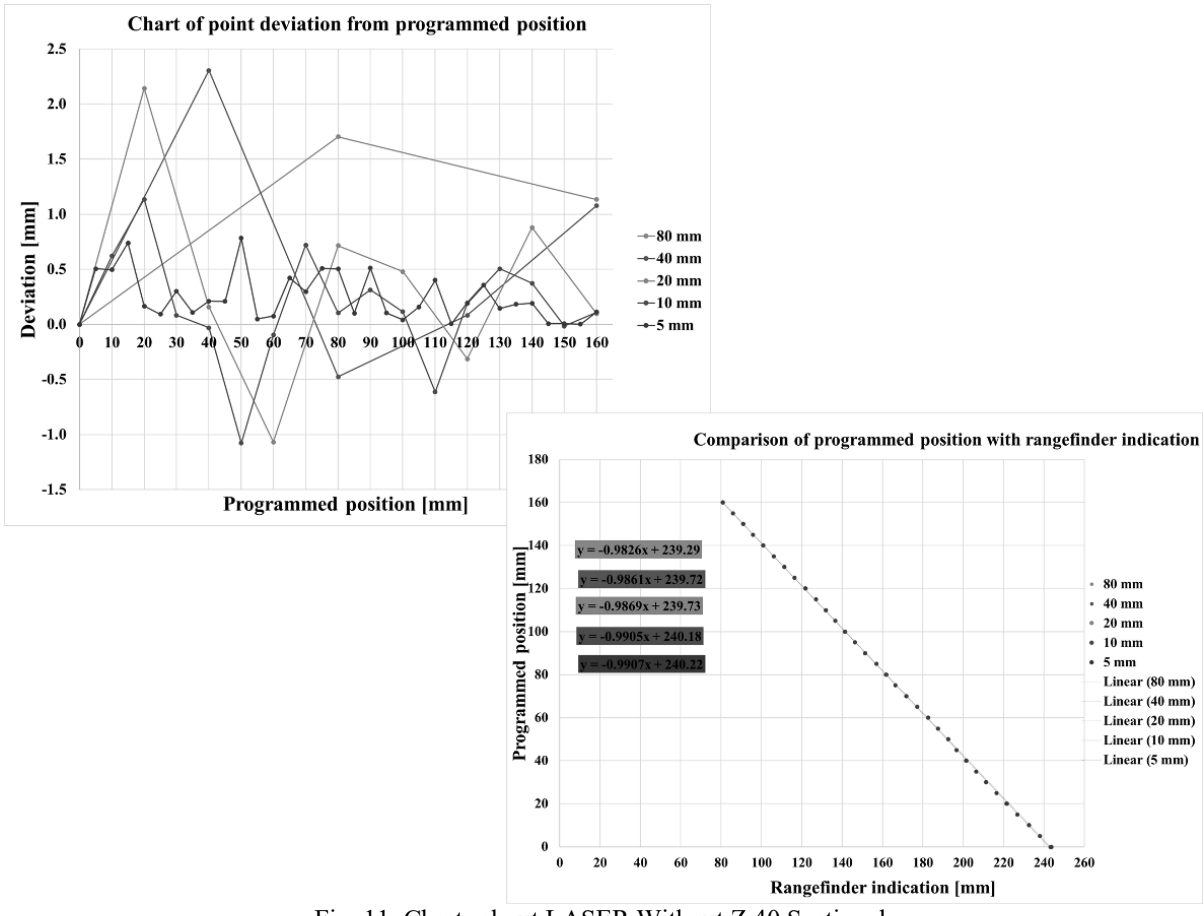


Fig. 11. Charts about LASER Without Z 40 Sectional.

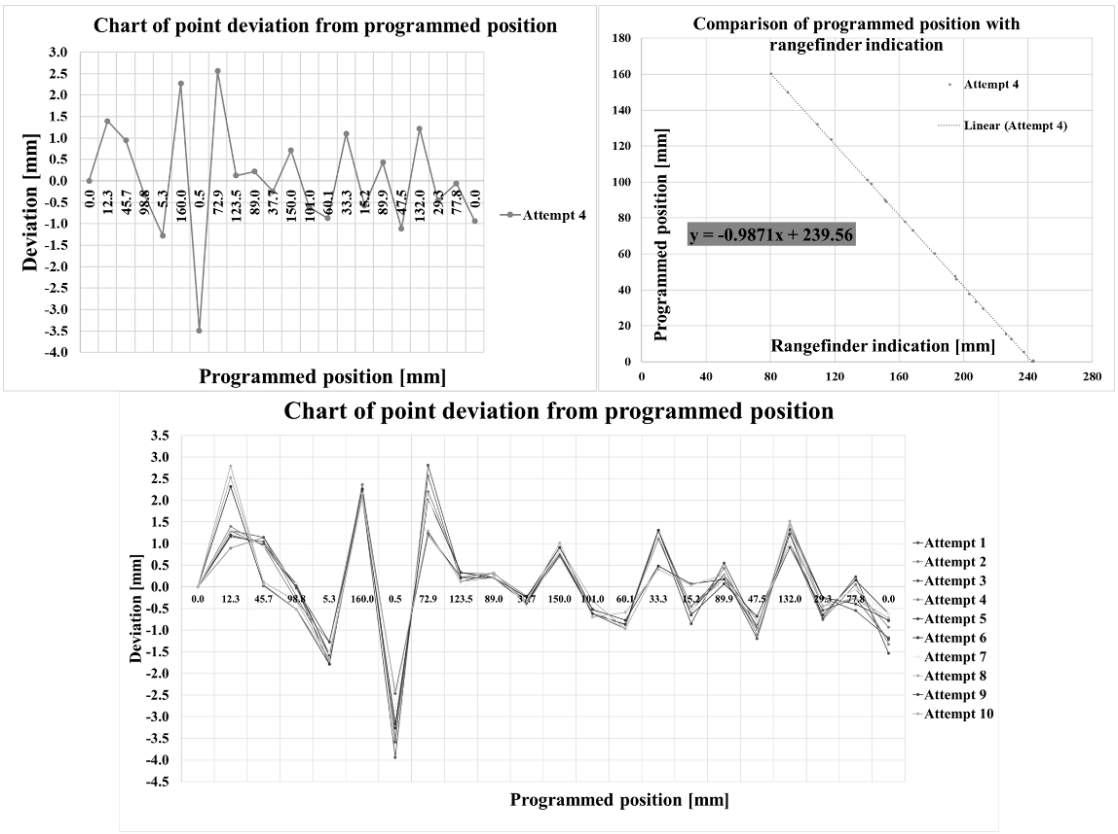


Fig. 12. Charts about LASER Without Z 40 Random.

For the X-axis in the LASER system, the best results were achieved at 39.65 steps/mm in Smooth mode, both in the no-load and loaded configurations. The average MEA error was significantly lower compared to the other modes, and the α angle difference remained <0.05°. Importantly, the maximum error values were also the lowest, and the standard deviation confirmed high repeatability. Figures 13 and 14 present the relevant data for the X-axis.

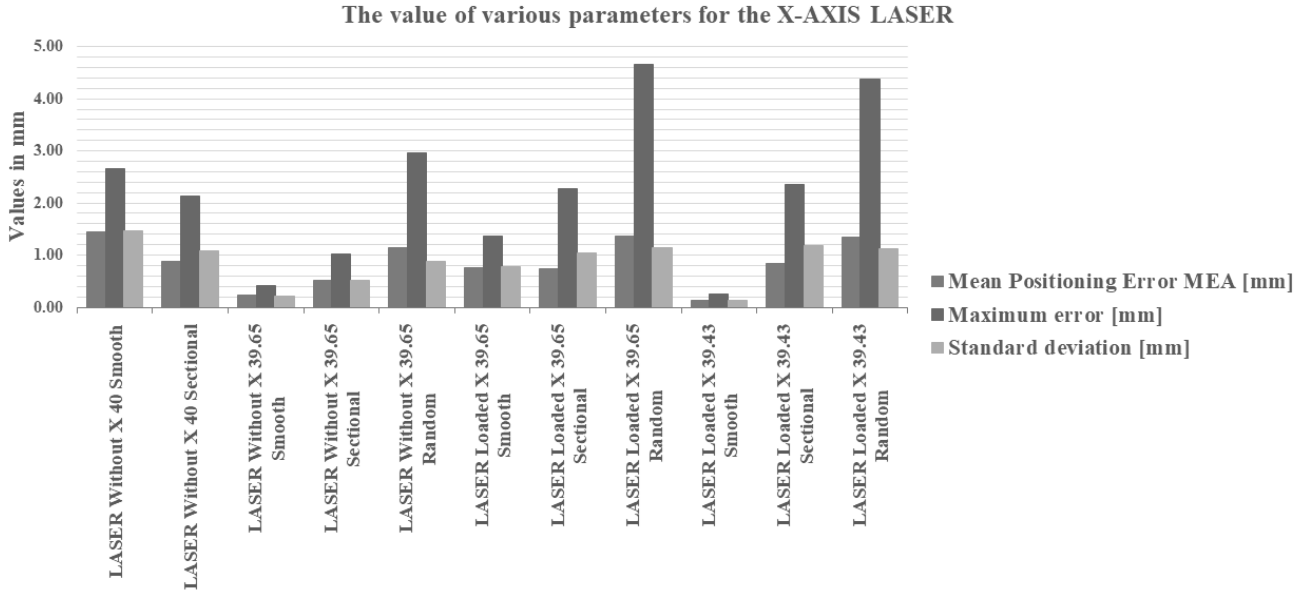


Fig. 13. Chart comparing data for the X-axis LASER system.

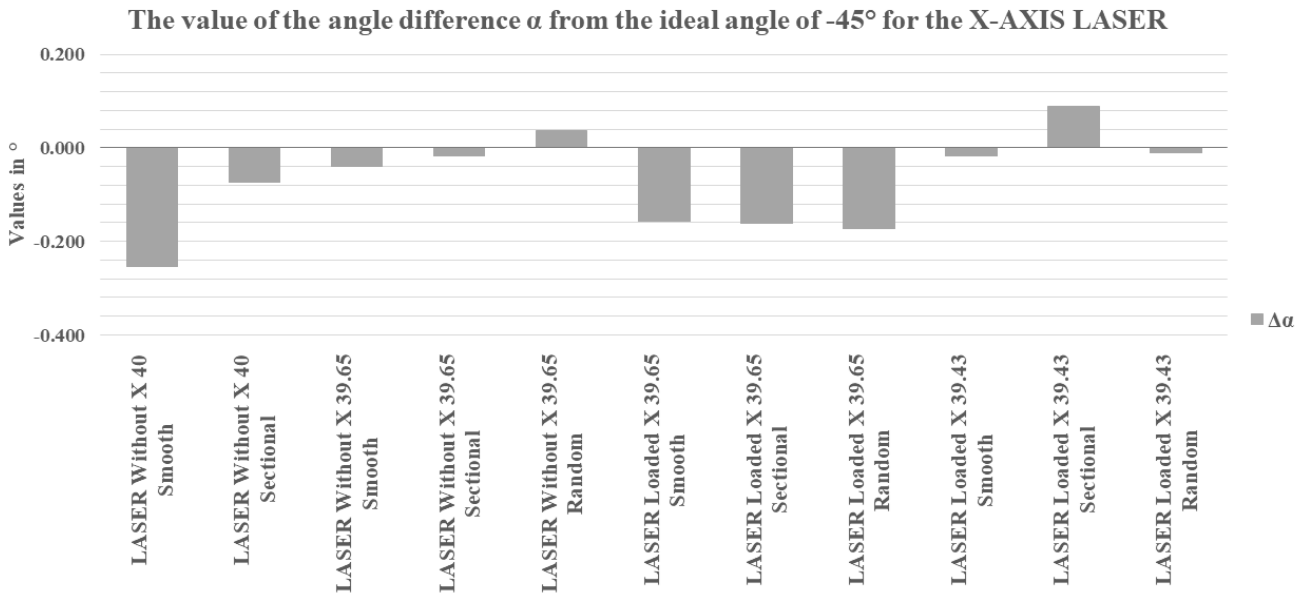


Fig. 14. Chart showing the differences α from the ideal angle of -45° for the X-axis LASER system.

The Y-axis in the same system showed greater variability of results, especially in the Random mode, where the MEA reached values of over 2 mm (in the 39.55 steps/mm parameter test, the average MEA was even 12.5 mm) and the Δα exceeded 1°. The maximum error in this case was significantly higher than in the other modes, and the increase in standard deviation indicated reduced stability of the system. The Smooth mode allowed for satisfactory parameters with steps/mm = 39.55. Figures 15 and 16 present the corresponding data for the Y-axis.

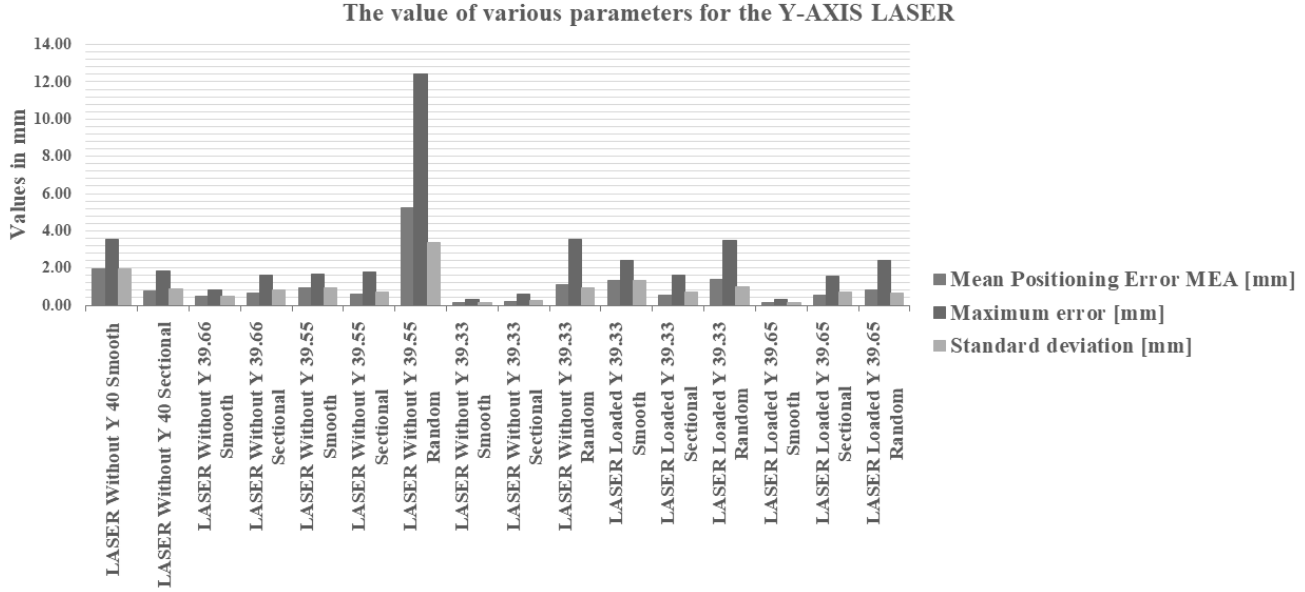


Fig. 15. Chart comparing data for the Y-axis LASER system.

For the Z axis, the results were the most stable. The differences between the modes were small, and Δα did not exceed 0.2°, which indicates that this axis is not susceptible to disturbances or positioning errors. The values of maximum errors and standard deviations were also among the lowest of all the analysed cases. Figures 17 and 18 illustrate the corresponding data for the Z-axis.

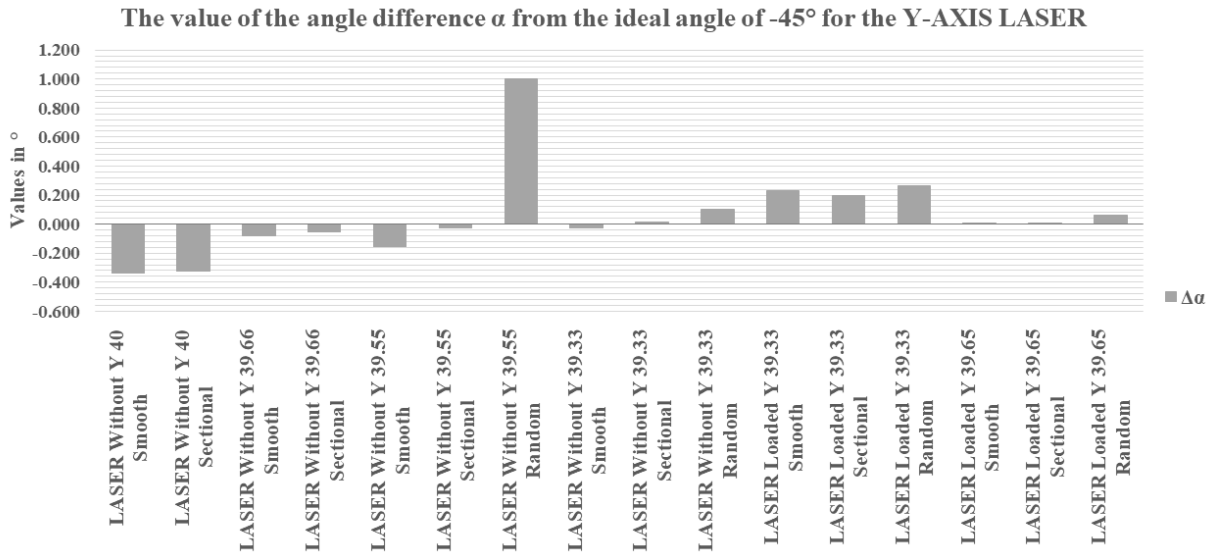


Fig. 16. Chart showing the differences α from the ideal angle of -45° for the Y-axis LASER system.

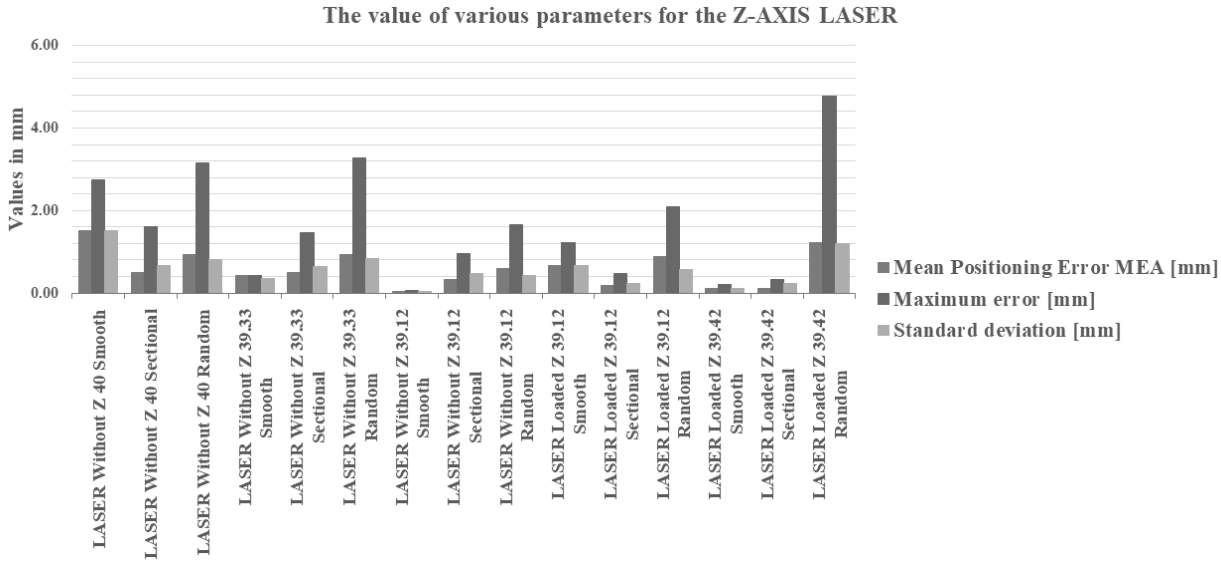


Fig. 17. Chart comparing data for the Z-axis LASER system.

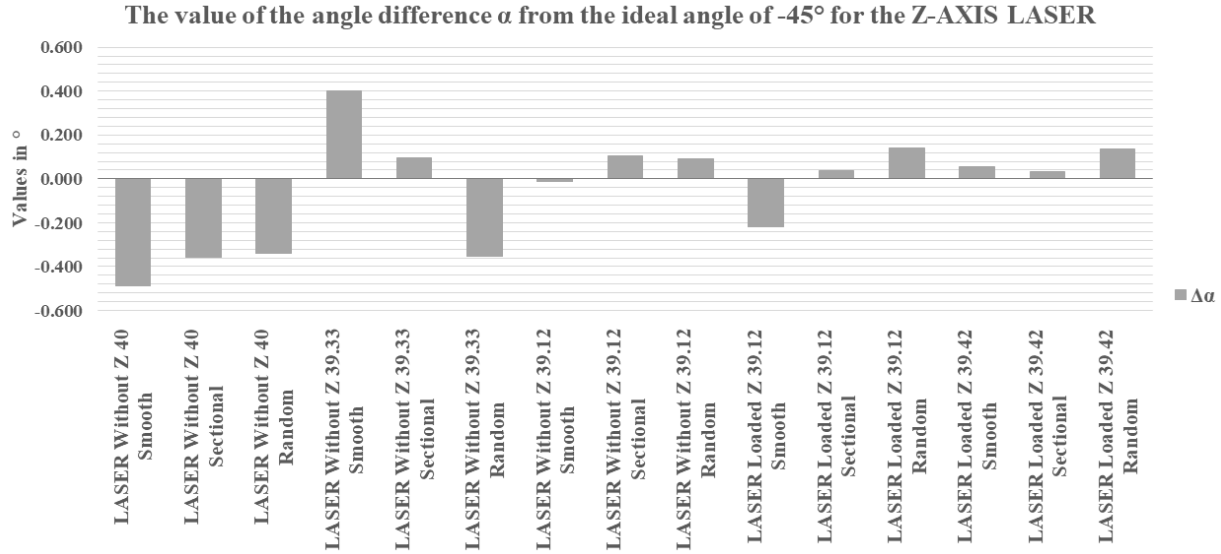


Fig. 18. Chart showing the differences α from the ideal angle of -45° for the LASER axis Z.

In the TEST system, the most stable results were obtained for the X-axis at steps/mm ≈ 39.59, Smooth and Sectional performed well, but the Random mode showed increased variability and an increase in Δα up to about 0.3°. The maximum errors were higher here, and the standard deviations indicated a greater dispersion of results. Figures 19 and 20 present the relevant data for the X-axis of the TEST system.

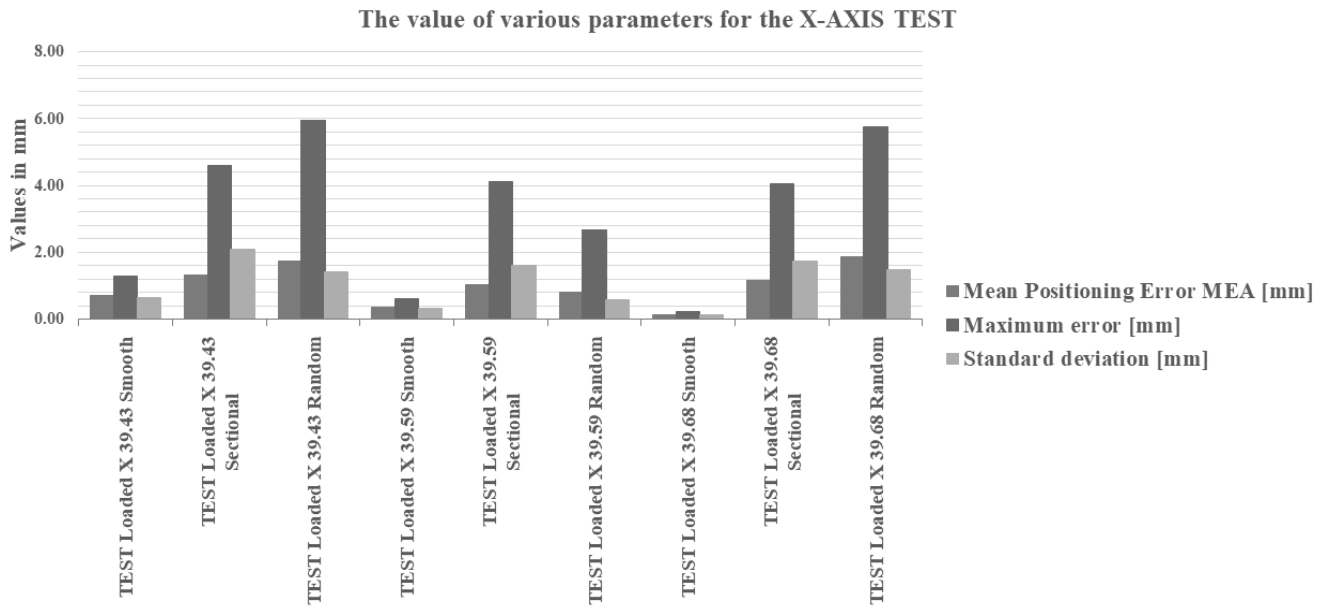


Fig. 19. Chart comparing data for the X-axis TEST system.

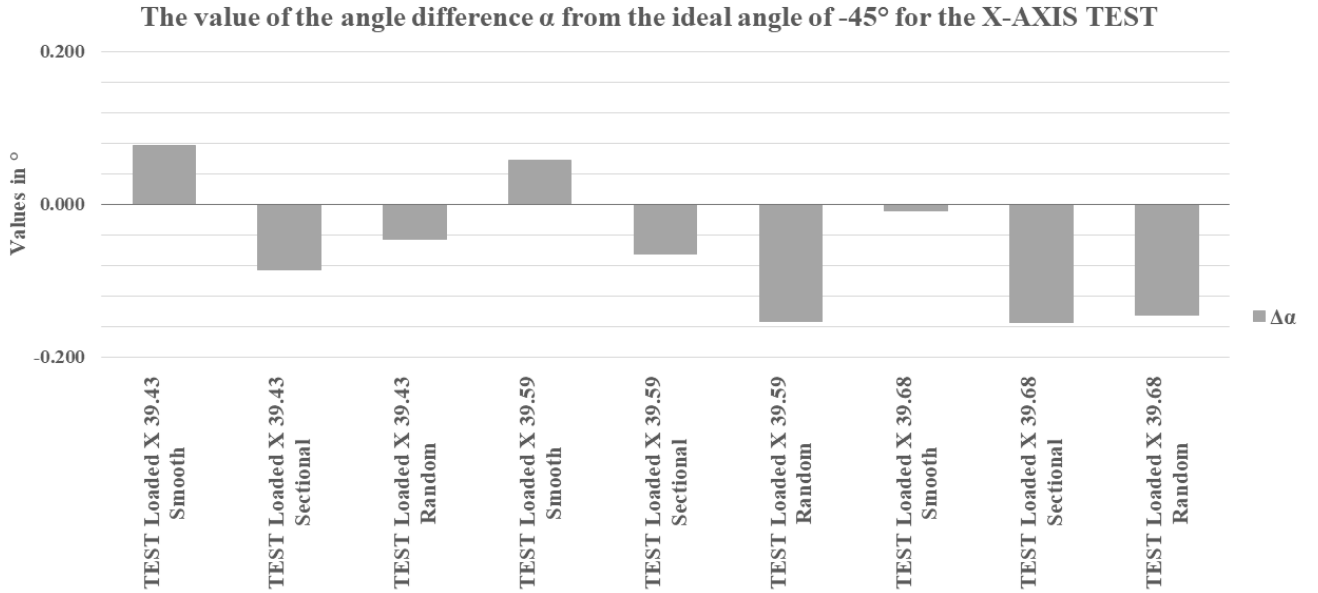


Fig. 20. Chart showing the differences α from the ideal angle of -45° for the X-axis TEST system.

Based on the measurements shown in Figures 21–24, the Y and Z axes were the most affected by the load. For the Y-axis, with steps/mm = 40.1, the MEA values increased notably in the Random mode, and Δα reached up to 0.9°. This was accompanied by a rise in maximum error and a significant increase in standard deviation. For the Z-axis, the data remained more consistent, although the mean error and maximum error were still higher than in the LASER system, while Δα stayed within acceptable limits.

To better understand the source of these deviations, a broader comparison of unloaded and loaded configurations was performed. In the LASER system, the MEA for the Y-axis increased from 0.15–0.47 mm to 1.35 mm, while Δα rose from below 0.05° to 0.23°. In the TEST system, the Z-axis reached Δα values up to 0.38°, showing that both axes respond noticeably to the additional 1.23 kg (laser module) and 2.5 kg (tester module). The load had the strongest effect on the Y-axis in the LASER system, while in the TEST system the Z-axis showed comparable sensitivity.

Structural optimisation therefore involves several practical modifications. The first step is to increase the stiffness of the Y-axis guides, for example by using a higher rail profile or a wider guide rail to reduce bending under the added mass. Another useful adjustment is a slight increase in carriage preload to minimise lateral play, which becomes most noticeable during longer travel distances in the Random mode. The final element is to stiffen the Z-axis mounting plate. The current plate is too thin and twists under load, which directly contributes to the increase in Δα. Using a thicker plate or a material with higher stiffness eliminates this deformation and stabilises the measurements under full load.

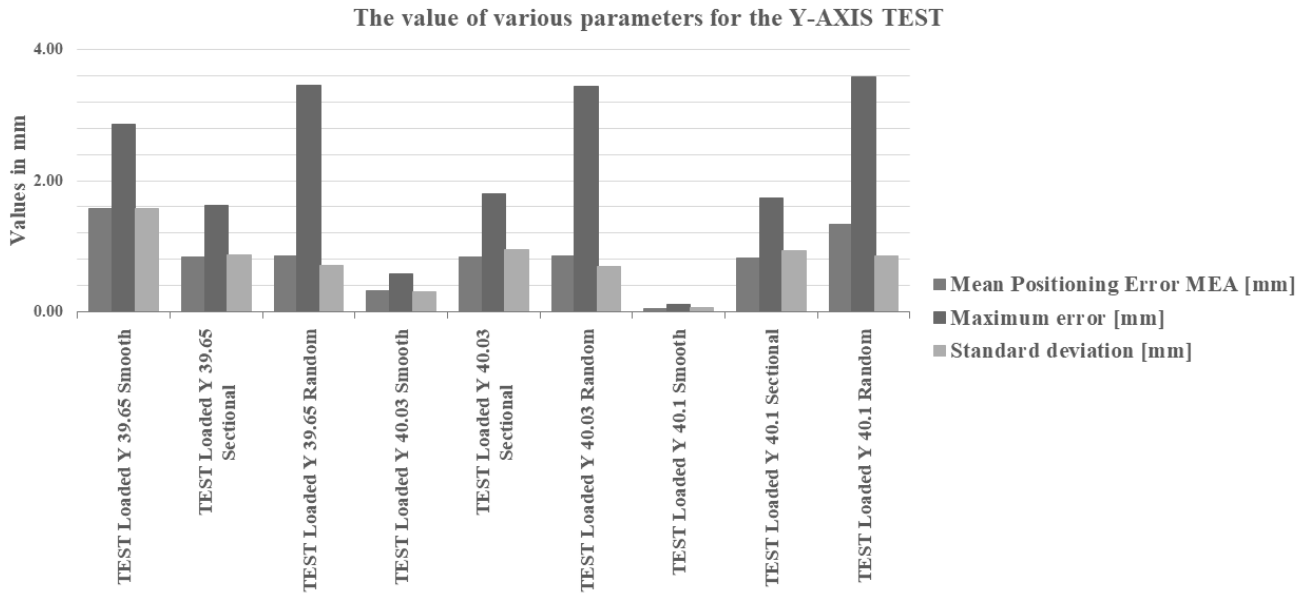


Fig. 21. Chart comparing data for the Y-axis TEST system.

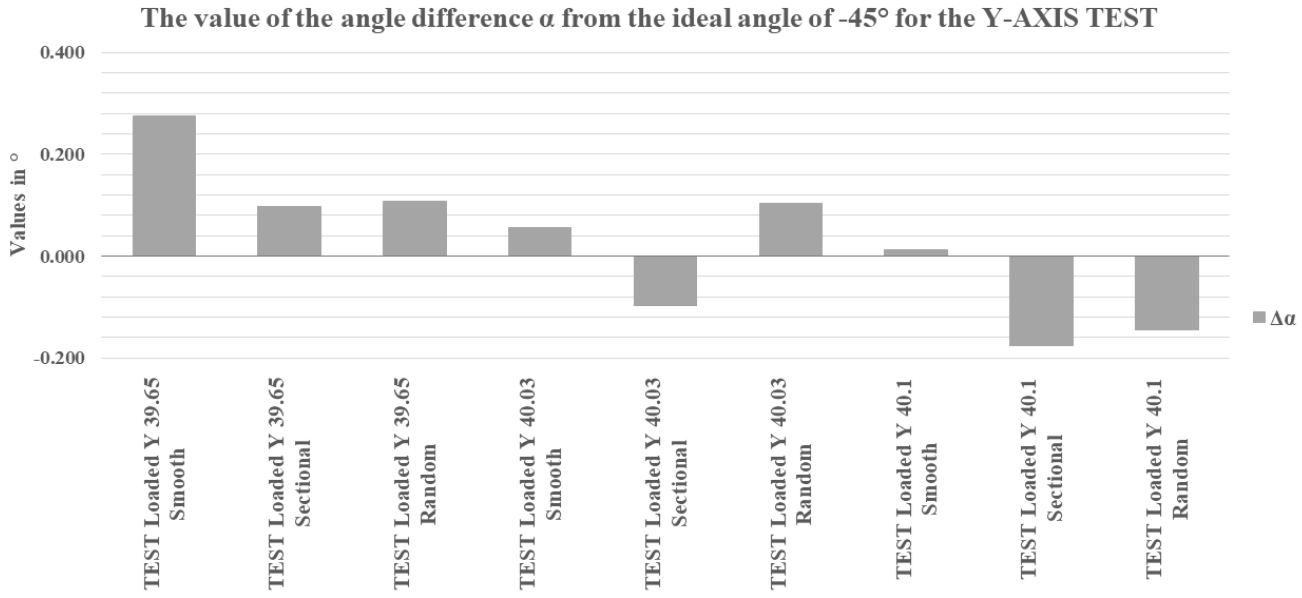


Fig. 22. Chart showing the differences α from the ideal angle of -45° for the Y-axis TEST system.

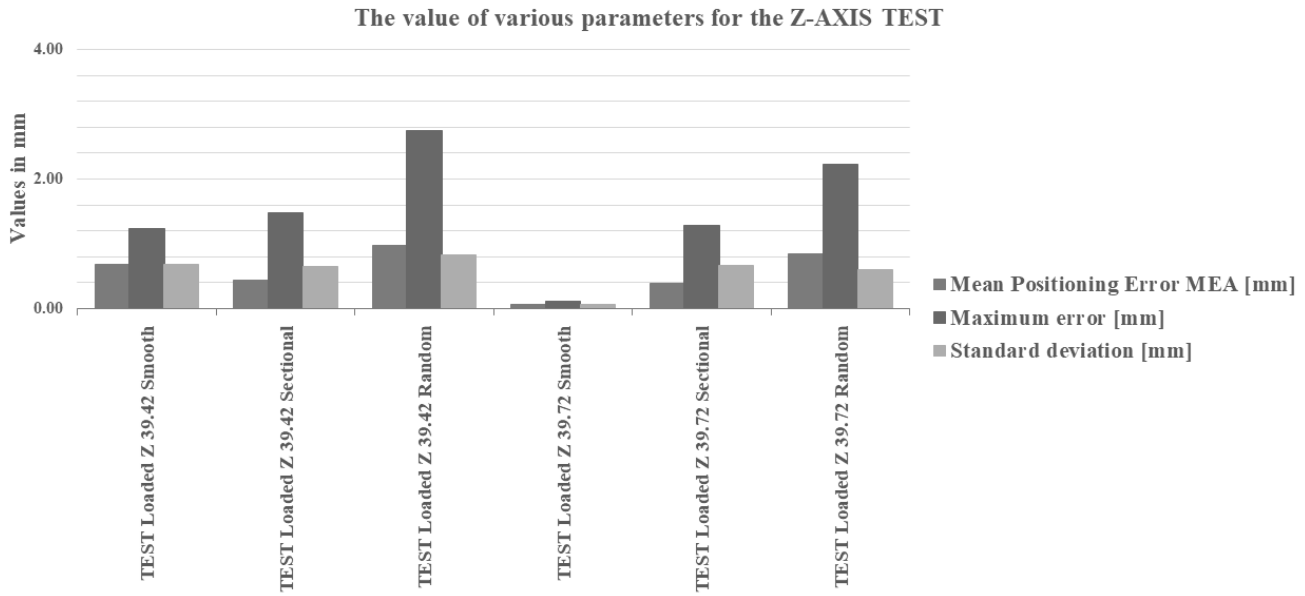


Fig. 23. Chart comparing data for the Z-axis TEST system.

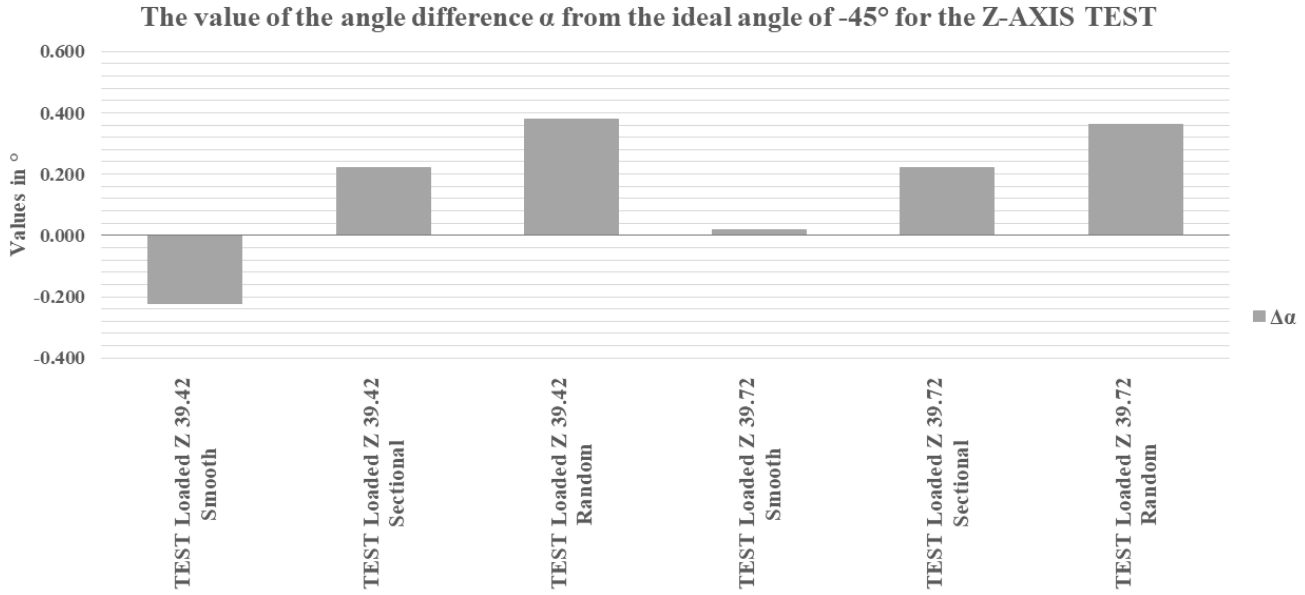


Fig. 24. Chart showing the differences α from the ideal angle of -45° for the Z-axis TEST system.

The Smooth mode proved to be the most effective in the calibration process. Sectional mode verified the correctness of this calibration. Random mode, on the other hand, tested the robustness of the system and the repeatability of movement. The load had a significant impact, primarily on the Y-axis in the LASER system and on the Z-axis in the TEST system. This confirms that further structural optimisation is required, especially in the guiding system of the Y-axis and in the mounting assembly of the Z-axis.

Overall, the Smooth mode provided the most reliable basis for calibration, the Sectional mode confirmed the correctness of the selected parameters, and the Random mode revealed the axes most sensitive to load and structural flexibility. These observations form the basis for the final conclusions presented in the next chapter. The load had the greatest impact on the Y-axis in the LASER system and on the Z-axis in the TEST system. The X-axis showed more variability mainly in Random mode, but was not the main component of the error.

## 4. CONCLUSION

Based on the research carried out, it can be concluded that the developed test and depanelization test rig is a valuable prototype of a mechatronic system that shows both its potential and its current limitations. The Smooth mode delivered the most stable and repeatable results, especially on the Y and Z axes. In the Random mode and under load, noticeably larger deviations appeared. The strongest influence of the load was observed on the Y axis in the LASER system and on the Z axis in the TEST system. The X axis showed increased variability mainly in the Random mode, but it was not the dominant source of errors and did not exceed the limits as consistently as the other two axes.

The source of problems can be mechanical clearance and the susceptibility of the system to vibrations - especially after the load is applied. Although the LEUZE laser sensor worked stably and did not raise any objections, the design of the system requires increased rigidity and a rethink of the centre of gravity. The limit sensors reacted to intense lighting, but under laboratory conditions this effect was negligible and did not affect laser measurements.

Despite the lack of vibration damping methods or extensive filtering algorithms, the results obtained in controlled modes (Smooth. Sectional) indicate that the system can be used as a demonstrator. The tests were carried out under laboratory conditions, but the analysis of standard deviations showed that the measurements were relatively stable and replicable. especially at low MEA values.

In the current version of the station, no vibration sensors were used, as the purpose of the test was to calibrate steps/mm and analyze the influence of the structure and load on positioning errors. In the next iteration of the prototype, it is planned to introduce vibration sensors when the structure is stiffened and it will be possible to study the dynamics of the entire system.

The final calibrated steps/mm values for all axes in both systems were consistent with the results obtained during the iterative optimisation process. In the LASER system (loaded configuration), the calibration converged to 39.43 steps/mm for the X-axis, 39.65 for the Y-axis and 39.42 for the Z-axis. In the TEST system, the final values were 39.68, 40.10 and 39.72 for the X-, Y- and Z-axes respectively. These values were determined through an iterative procedure aimed at minimising the MEA, standard deviation and $\Delta\alpha$, confirming the stability and repeatability of the calibration process as well as the mechanical similarity between both setups.

**Author Contributions:** Conceptualization: M. Łyczek; Methodology and implementation: M. Łyczek; Supervision: W. Skarka; Writing—original draft: M. Łyczek; Review and editing: W. Skarka.
**Funding Source:** The research was supported internally by AIUT Sp. z o.o. This research was co-financed by the Ministry of Science and Higher Education. the Republic of Poland within the "Doktorat wdrożeniowy" program. sixth edition 10/060/SDW22/2032. The publication was supported by the statutory funds of the Silesian University of Technology.
**Conflicts of Interest:** There is no conflict of interest.

## REFERENCES

[1] S. Silvestre Bergés, J. Salazar Soler, J. Marzo, (2019), *Printed Circuit Board (PCB) design process and fabrication*, Publisher Czech Technical University of Prague. Faculty of Electrical Engineering, available at: https://hdl.handle.net/2117/134361

[2] M. Łyczek i W. Skarka, (2024), *Review of Methods for PCB Panel Depanelization and Methods for Correct Assembly of Electronic Components on PCB Panels*, Electronics, 13(7):1255, doi: 10.3390/electronics13071255.

[3] P. Lerma, (2014), *Design Practices for panelization and depanelization*, Printed Circuit Design and Fab/Circuits Assembly, 31(6), 22–25.

[4] H. van Schaaijk, M. Spierings, E. J. Marinissen, (2018), *Automatic Generation of In-Circuit Tests for Board Assembly Defects*, IEEE International Test Conference in Asia (ITC-Asia), pp. 13–18, doi: 10.1109/ITC-Asia.2018.00013.

[5] S. L. Jurj, R. Rotar, F. Opritoiu, M. Vladutiu, (2020), *Affordable Flying Probe-Inspired In-Circuit-Tester for Printed Circuit Boards Evaluation with Application in Test Engineering Education*, IEEE International Conference on Environment and Electrical Engineering and 2020 IEEE Industrial and Commercial Power Systems Europe (EEEIC / I&CPS Europe), pp. 1–6, doi: 10.1109/EEEIC/ICPSEurope49358.2020.9160639.

[6] M. Sikora, M. Grochowski, (2011), *Wykorzystanie sieci neuronowych do diagnostyki poprawności wykonania płytek drukowanych*, Pomiary Automatyka Robotyka, 15(2), 49–54.

[7] M. Alghassab, (2021), *Defect Detection in Printed Circuit Boards with Pre-Trained Feature Extraction Methodology with Convolution Neural Networks*, Computers, Materials and Continua, 70, 637–652, doi: 10.32604/cmc.2022.019527.
[8] B. Russell, (2005), *Verifying flying prober performance - fitness is survival*, IEEE International Conference on Test, pp. 17–24, doi: 10.1109/TEST.2005.1583958.
[9] Adrian, (2025), *The Bed-of-Nails Advantage: Maximizing Test Coverage with ICT Fixtures,* Available at: https://www.allpcb.com/blog/pcb-assembly/the-bed-of-nails-advantage-maximizing-test-coverage-with-ict-fixtures.html
[10] ***(2021), *Test probes – types and application,* available at: https://www.tme.eu/en/news/library-articles/page/43763/test-probes-types-and-application/, accessed March 29, 2025.
[11] G. D. Mysore, J. M. Conrad, B. Newberry, (2006), *A Microcontroller-Based Bed-of-Nails Test Fixture to Program and Test Small Printed Circuit Boards*, Proceedings of the IEEE SoutheastCon 2006, 104–107, doi: 10.1109/second.2006.1629332.
[12] R. Shannon, G. Zucaro, J. Tallent, V. Collins, J. Carswell, (2019), *A system for detecting failed electronics using acoustics*, IEEE Instrumentation & Measurement Magazine, 22(4), 32–37, doi: 10.1109/MIM.2019.8782197.
[13] D. Stewart, (2003), *Interconnect stress testing (IST) – an overview of its development and capabilities*, Circuit World, 29(2), 20–26, doi: 10.1108/03056120310454961.
[14] R. Basniak, M. Fontana Catapan, (2012), *Design of a PCB milling machine,* ABCM Symposium Series in Mechatronics, 5, 1339–1348, available at: https://www.abcm.org.br/symposium-series/SSM_Vol5/Section_VIII_Sensors_and_Actuators/10991.pdf
[15] K. Fathima, V. J. Shilpa, S. H. Mahmood, M. Lahari, (2018), *Design and Implementation of Three-Axis Cost Efficient CNC PCB Milling Machine*, International Conference on Recent Trends in Electrical, Control and Communication (RTECC), 106–109, doi: 10.1109/RTECC.2018.8625647.
[16] A. Oosterhof, (2016), *Material effecty of laser energy when processing circuit board substrates during depaneling*", SMT Surface Mount Technology Magazine, 31(7), 90–100.

Received: March 22th, 2025 / Accepted: November 18th, 2025 / Paper available online: December 20th, 2025